Self-Assembled Nanoparticle Necklaces Network Showing Single-Electron Switching at Room Temperature and Biogating Current by Living Microorganisms

Jennifer Kane, Mehmet Inan, and Ravi F. Saraf*

Department of Chemical and Biomolecular Engineering, University of Nebraska-Lincoln

ABSTRACT A network of one-dimensional (1D) Au nanoparticle necklaces is synthesized and shown to exhibit electronic switching, that is, gating, by the metabolic activity of yeast cells deposited on the structure. Without the cells, the network exhibits the Coulomb blockade effect at room temperature with a sharp threshold voltage, V_T of ~0.45 V, which corresponds to a switching energy of ~20 kT. Although the enhancement in V_T from ~70 mV for a single (10 nm) Au particle to >1 V is well-known for a 2D array, the uniqueness of the network topology is the relatively weak dependence of V_T on temperature that leads to room temperature switching behavior, in contrast to an array where the blockade effect vanishes at ambient temperatures. The coupling between the biochemical process of the cell and the electronics of the network has potential applications for making electrodes for biofuel cells and highly sensitive biosensors using the cell as the specific sensing moiety.

KEYWORDS: nanodevices · Coulomb blockade · single electron devices · critical phenomena · granular system · nanoparticle array

A possible approach to building a hybrid bionanodevice that is powered or regulated by a microorganism is to electronically couple it to a nanodevice sensitive to the production of a few electron charges from the cell due to its biochemical activity, and the nanodevice is chemically nontoxic to the cell. A single nanoparticle behaves as a robust standalone switch such that the current through it can be modulated by a single electron altering the charge (or discharge) state of the particle.[1] Transistors and logic devices which use a single nanoparticle have been demonstrated to modulate current using that single nanoparticle.[2,3] The key parameter of the device is the Coulomb blockade voltage, V_T, above which the current switches on, that is, suddenly begins to increase.[1] The current is turned ON when the Coulomb blockade is overcome due to a single electron charge of barrier energy, eV_T, where e is the charge of an electron.

The nanoparticle−microorganism system seems ideal for building hybrid bionano-electronic devices where the (few) redox electrons from a cell or microorganism can, in principle, modulate the current through the particle by altering the charge state of the nanoparticle. However, cryogenic temperatures are required for these single-particle, single-electron devices since the barrier energy for switching, eV_T, is small, <100 meV, for a typical 10 nm Au particle.[1] Coulomb blockades at room temperature can be obtained by a single particle <1 nm;[4] however, quantum noise and charge fluctuation make the devices very noisy.[5,6]

The switching voltage, V_T, and the corresponding switching barrier energy, eV_T, can be enhanced by over an order of magnitude using a two-dimensional (2D) array of nanoparticles. In recent years, on the basis of theoretical predictions,[7] 2D arrays of nanoparticles that are easy to interconnect with electrical circuits have been demonstrated to exhibit similar switching behavior[8−10] and robust V_T above 1 V. Using some aspects of self-assembly, several top-down approaches, such as utilization of thiol-ligated Au nanoparticles,[11−14] assembly at the solvent-air interface,[15,16] and a live bacterium surface,[17] have been developed to fabricate 2D arrays interconnected to circuitry. Unfortunately, the over 10-fold enhancement compared to a single nanoparticle caused by several Coulomb blockades over the percolation path in the array vanishes at room temperature because V_T decreases (linearly) as temperature, T, increases.[8,18]

*Address correspondence to rsaraf@unlnotes.unl.edu.

Received for review June 3, 2009 and accepted November 05, 2009.

Published online December 28, 2009.
10.1021/nn901161w

Although not studied for its Coulomb blockade properties (and subject of this report), an alternative architecture is a monolayer of 1D array of particles. A 1D array can be made using three possible approaches. Clusters of 1D arrays are synthesized by mineralization of (usually noble) metal from salt precursors or seed on a variety of 1D templates, such as DNA,[19] peptides,[20] nanotubes,[21] and polyelectrolytes,[22] to form a broad size distribution of particles, either discrete or continuous nanowires. In the second method, (monodispersed) nanoparticles are self-assembled on templates, such as CNT,[23] DNA,[24,25] polysaccharide,[26] and peptide microfibrils,[27] to form a discrete (*i.e.*, insulating) 1D array. In the third method, an intrinsic magnetic[28] or electric[29] dipole, or induced electric dipole, of the particle is used to self-assemble 1D necklaces of nanoparticles. The electric dipole can be induced by either replacing the immobilized ionic moiety with a neutral species[30] or partially neutralizing the charge with mobile ions.[31,32] In the third method, the particles are in close proximity for electron tunneling which is manifested as red shift in surface Plasmon absorption spectrum[30] and non-ohmic conductivity of the 3D network (*i.e.*, several monolayers) deposited between electrodes.[31] Although the optical application of "Plasmon wave guide" aspect of the necklace is well reported,[33] the (interesting) electrical properties of monolayer of 1D necklaces are not as recognized.

This report describes a novel architecture composed of a 2D network (*i.e.*, monolayer) of 1D nanoparticle necklaces of 10 nm Au particles where, for the first time, robust single-electron switching, that is, V_T, is observed at room temperature. Necklaces of nanoparticles were self-assembled in solution by an induced electric dipole mediated by ions and deposited on solid substrate to form a well over 1 mm large 2D network (*i.e.*, monolayer) of 1D Au nanoparticle necklaces. Unlike the previous study[31] that used a 3D network mediated by Cd^{2+}, a toxin to living cells, the reported study is a 2D network mediated by H^+ ions. The room temperature switching occurs because, unlike the 2D (ordered or disordered) array, V_T becomes nominally independent of T above 50 K for this necklace architecture. The robust V_T at room temperature and nontoxic nature of the necklace allows the possibility of developing a hybrid bionanodevice with living cells. Biogating the necklace network by depositing live yeast cells is demonstrated. As the cells are fed a nutrient (methanol vapor), the metabolic activity modulates the current through the network.

RESULTS AND DISCUSSION

Assembly of the necklace network begins with a wine red suspension of citrate-functionalized 60 and 10 nm Au particles (Figure 1a). Upon the slow addition of HCl to the particle suspension, the H^+ ions compensate the immobilized negative charges on the particle

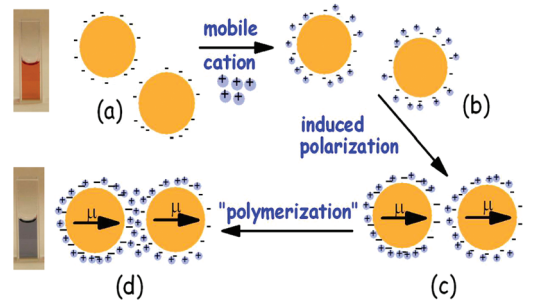

Figure 1. Polymerization of nanoparticles to form a 1D necklace. (a) The negatively charged Au nanoparticles, stabilized in water at pH ~7, have a nonuniform charge distribution due to faceted crystal planes that have different affinities for citrate ions. (b) On addition of H^+, some of the negative charges are compensated. (c) When these particles come close during thermal motion, they induce a dipole moment and cause an attractive interaction. (d) When the induced dipole is strong enough, the particles bond to form a 1D necklace with the dipoles aligned. The cuvettes show the color of the Au nanoparticle suspension before and after necklace formation.

(Figure 1b). The pH of the Au suspension on addition of HCl reduces from ~6 to 2.7. The details of the procedure are described in the Supporting Information. Below a pH of 2.5, the solution becomes unstable; and above a pH of 3, only small clusters of 2−5 particles are deposited. Analogous to previous reports,[31] electric dipole is induced by an asymmetric accumulation of H^+ ions. The high surface mobility of the H^+ ions on the particle surface induces an electric dipole when the particles come close together during thermal collision (Figure 1c). When the attractive force between the induced dipole is larger than ~kT, the particles bond such that the dipoles align and "polymerize" the particles into a long 1D necklace that is manifested as a change in color of the suspension to violet blue (Figure 1d). Owing to the slow collision rate, the formation takes ~18 h. The change in color is due to red-shift in the surface plasmon resonance in the nanostructure (see Supporting Information, Figure S1).[30] Although not understood, the inclusion of 60 nm Au nanoparticles in the solution significantly increases the necklace formation kinetics and results in a solution that is stable for well over 1 week.

The device is made by simply adsorbing the necklace onto a Si chip passivated with 500 nm thick thermal oxide and 300 nm thick Au electrodes at 10 and 20 μm spacing. On each of the 20 chips studied, there are five devices each. All of the chips exhibit conduction for ~5 mm channel width. However, after removing part of the necklace by scratching with an STM tip to make a 1−0.1 mm wide channel, the nonlinearity improves significantly; but 20% of the devices become an open circuit due to nonuniformity in deposition and possible defects during scratching. The remaining 80% exhibit non-ohmic behavior (discussed below in Figure 3). The deposition is reasonably uniform with the necklaces forming a highly branched network made up of 1D in-

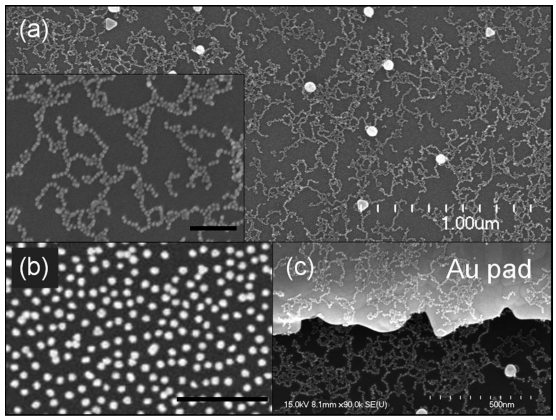

Figure 2. Field emission scanning electron microscope (FESEM) image of the network deposited on a SiO_2/Si chip. (a) The necklace deposition after exposing the chip to the solution for ~24 h. (b) Deposition of pure 10 nm particles from the pH 7 solution. (c) The deposition of the necklace on the Au pad is good leading to a naturally robust interconnection with the array. (Inset a) Higher magnification image of the nanoparticle necklace. The scale bar in inset a and panel b is 100 nm.

dividual strands (Figure 2a). The 60 nm particles do not appear to have any particular correlation with the necklace structure. In contrast to the 48-h deposition of charge-stabilized (as-received) 10 nm particles (Figure 2b), which are sparse (and nonpercolating) because of electrostatic repulsion, the network of necklaces forms long-range percolating channels traversing over tens of micrometers with good contact to electrodes (Figure 2c) after a deposition time of ~24 h. Electrostatic repulsion between the necklace segments makes the percolating network highly exfoliated.

$I-V$ behavior of a network deposited between electrodes spaced at 20 μm exhibits no hysteresis over several cycles and is highly symmetric (Figure 3a). After 30 cycles, there is some decrease in V_T; however, the symmetry in forward and reverse bias is maintained with no hysteresis (Figure S2 in Supporting Information). Consistent with other studies on 2D nanoparticle arrays,[8,18] the I reduces as the T decreases; and the nonlinear $I-V$ characteristics exhibit a conspicuous V_T at subambient temperatures. The $I-V$ behavior of a nanoparticle array is analogous to a second order phase transition given by $I \approx [(V - V_T)/V_T]^{\zeta}$, where the critical exponent ζ for 2D arrays is analytically determined to be $^5/_3$.[7] There is excellent agreement with the scaling law with a universal ζ of $^5/_3$ for the full temperature range of study, 5−295 K (Figure 3b). To ensure the robustness of the data, one to three $I-V$ cycles are measured at each temperature. The V_T is estimated from the raw data using a nonlinear curve fitting method (see Figure S3 in Supporting Information). The data for 15, 35, and 150 K is taken during cooling while the rest are measured during heating from 5 to 295 K.

The central difference (and the novelty of the reported structure) compared to 2D nanoparticle arrays is in the behavior of V_T as a function of T. At low temperatures, the linear decrease in V_T with increasing temperature is similar to other 2D array studies;[8,18] however, a sharp change in slope occurs around 50 K (Figure 4a). Above 50 K, similar to a single nanoparticle, the V_T becomes a weak function of T. As a result, for a 10 μm gap, high V_T of ~0.45 V at room temperature is obtained (Figure 4b). The corresponding switching energy, eV_T, at room temperature is ~20 kT. This is an approximately 10-fold enhancement compared to a single particle blockade. The raw data explicitly exhibiting V_T at room temperature is shown in Figure S3 of the Supporting Information.

The sharp transition at 50 K for both gaps is attributed to the topology of the percolation path in the necklace network array. Field emission scanning electron microscope (FESEM) images (Figure 2a) indicate exfoliated necklace network morphology that is locally a 1D conductor with branching points several nanoparticles apart. Therefore, the coordination number for the necklace network is about 2, in contrast to a dense, randomly close-packed 2D array of 4−6. Simulation studies on dense 2D arrays show that as the bias rises from 0 to V_T, the array increasingly charges with single-electron charges trapped in some of the individual nanoparticles that are randomly distributed over the

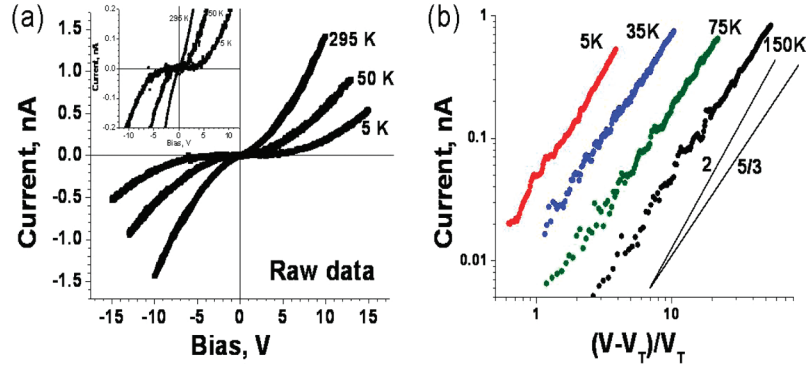

Figure 3. $I-V$ characteristics for the 20 μm gap. (a) Raw data at three temperatures for the same sample. The voltage ramp is 0 to positive to 0 to negative to 0 V. The width of the necklace network is 100 μm. The inset shows a magnified view to illustrate the blockade characteristics. (b) The raw data is replotted as $[(V - V_T)/V_T]$ *versus* I. The lines with slopes of 2 and $^5/_3$ are shown for comparison.

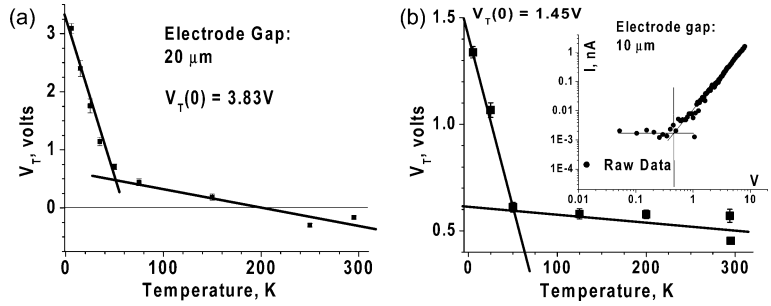

Figure 4. Effect of temperature on V_T. (a) For the 20 μm gap, V_T as a function of T shows an abrupt change in slope at ~50 K and has a $V_T(0) = 3.83$ V. V_T becomes <0 above ~200 K indicating no switching behavior at room temperature. (b) For the 10 μm gap, V_T as a function of T also shows an abrupt change in slope at ~50 K. The significantly smaller slope at $T > 50$ K leads to a V_T of ~0.45 V at room temperature. The inset shows raw data at 295 K to explicitly indicate the Coulomb blockade effect at room temperature.

array.[7,34] As the $I-V$ current exhibits no hysteresis (Figure 3a), this random charge distribution is fixed, that is, quenched, as also observed for nanoparticle arrays.[10,18] In well-developed theory on 2D arrays of nanoparticles, random quenched charge distribution[7,34] presents barricades to the percolation path that are overcome as the bias gradually increases. Owing to a large coordination number in the dense 2D array, the percolation path is optimized to reduce the number of barricades (of energy height ~e/2C) in their trajectory.[7] As the temperature increases, some of these barricades are washed out because of the higher energy of the conduction electrons. This leads to a linear decrease in V_T such that at some $T \geq T^*$, there is at least one percolation path with no barricade connecting the two electrodes, resulting in no Coulomb blockade (*i.e.*, $V_T \leq 0$).[18] Consistent with experimental observations, this model predicts a linear decay of V_T as T increases.[18] T^* for a dense 2D array is below room temperature. In contrast, the 1D necklace network geometry constricts the percolation path due to a lower coordination number. Thus, the (fewer) barricades that still survive at high temperature in the percolation path cannot be circumvented due to the low coordination number of the array, hence a higher V_T is expected.

The barrier height of the barricade is the energy used to charge the isolated single particle (or cluster) with a single electron.[7,18] For a 10 nm particle surrounded by dielectric media of $\epsilon \approx 4$, the capacitance is 2.22×10^{-18} F. The potential rise due to single-electron charging is $e/C \approx 72$ mV that presents an energy barrier of 72 meV. A doublet, that is, two particles in physical contact with a tunneling barrier well below kT, has a $C \approx 3.1 \times 10^{-18}$ F and an energy barrier of 51 meV. For a reasonable Coulomb blockade, or barricade, the barrier should be ~$10kT$,[1] thus a doublet with a barrier energy of ~$12kT$ at 50 K presents a barricade to electron transport. Therefore, for $T < 50$ K, doublets and clusters larger than a doublet can also store charge to present a barricade. Because the barricade cannot be circumvented in the necklace network, due to a low-coordination number, as T decreases beyond 50 K, the contribution from larger (individual) clusters increases, contributing to the rapid increase in V_T. However, for $T > 50$ K, the barricades will only be limited to single nanoparticles imbedded in the necklace segments. In other words, above 50 K, the 1D necklace segments in the percolation path are punctuated with nanoparticles with trapped single-electron charge that present a barricade to the electron flow (Figure 5). The transition at 50 K is sharp because the barricade size abruptly rises from a single particle (the majority of barricades) to the contribution from the cluster of two particles.

The model is identical to the classical models for 2D arrays.[7,34,35] The only difference is that the conduction is through well-defined percolation paths made up of 1D necklace segments. As the bias ramps up, the current rises rapidly as barricades are overcome, leading to more possible network pathways for electron percolation. For example, in Figure 5 at low bias, only the "blue" pathway is "open" as it has the least amount of barricade; as the bias increases, the "red" pathways also become "open" leading to a rapid rise in current.

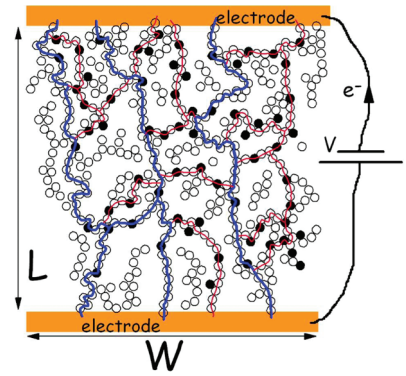

Figure 5. Schematic of an L by W, 2D array of nanoparticle necklace showing percolation channels connecting the source and drain electrode. The dark circles are particles with "quenched" single electron charge (see text) that act as barricades to the electron flow due to external bias, V. The percolation channels are defined by the topology of the network and are locally 1D. Channels containing lower linear density of barricades (blue) will percolate at a lower bias than the paths with a larger number of charged particles (red).

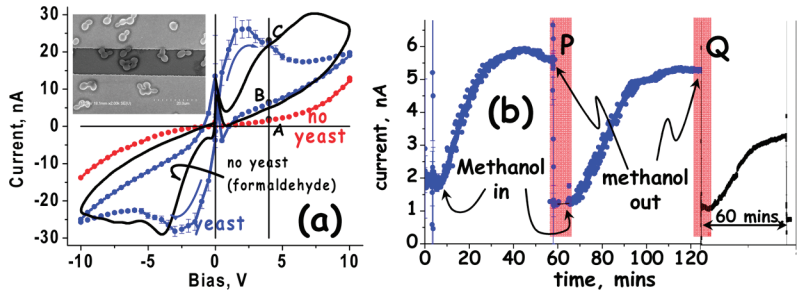

Figure 6. Biogating of the nanoparticle necklace device with the metabolism of living microorganism cells. (a) The *I*−*V* behavior of the necklace network on exposure to methanol. Two curves with data points correspond to the network as is (no yeast) and with discrete yeast cell deposition on exposure to methanol. The solid line is the response of the network as is, without yeast, on exposure to formaldehyde. The inset shows an FESEM image of yeast cells on the network between 10 μm spaced Au electrodes. (b) The modulation of device current at 4 V as the yeast cell is exposed to methanol. At points P and Q, the methanol is removed.

For the single isolated nanoparticle barricades at $T > 50$ K based on 2D array theory, the effective charging energy of the array is $\sim eV_T(0)/\alpha N$, where N is the length of the conduction path in number of particles and α is a parameter that accounts for the quenched charge density stored in the array.[7,10,34] The α parameter for dense 2D arrays is experimentally measured to be $\sim$0.25,[10] which agrees well with simulation calculations that predict α in the range of 0.23 to 0.36 depending on the lattice geometry of the array.[7,34,35] In the necklace network, for an electrode gap of 20 μm, $N \approx$ 2000 (at least), leading to $\alpha \approx eV_T(0)/[N(e^2/2C)] \approx 0.002$, where $V_T(0) \approx 0.65$ V (extrapolated from $T > 50$ K behavior to 0 K in Figure 4a). The over 100-fold smaller α for a necklace network compared to a dense lattice indicates an open structure with few trapped charge centers, or barricades, leading to (most importantly) a smaller T *versus* V_T slope above 50 K, as observed in Figure 4. A consequence of smaller slope at $T > 50$ K allows for the possibility of obtaining a robust Coulomb blockade effect at room temperature for the 10 μm gap (Figure 4b).

Next, the "living" biotransistor is demonstrated. Owing to V_T at room temperature, biogating on the 10 μm devices is explored. The electrochemical coupling between the metabolic process of the living cell, *Pichia pastoris* (yeast), and the necklace is obtained by simply depositing, or seeding, the cells on the device by immersing the device in the cell suspension followed by washing. The $\sim$2 μm diameter yeast cell, *P. pastoris*, can survive in air for approximately 14 h, as long as humidity is maintained above $\sim$70%. The cells are grown in media containing methanol as a carbon source for 24 h. About 200 yeast cells are then deposited on an $\sim$1 mm wide nanoparticle necklace network (Figure 6a, inset).

First, the effect on the *I*−*V* behavior in the yeast-network coupling due to metabolism in the cell is considered. The *I*−*V* after deposition of the cells does not change significantly. Upon exposure to methanol vapors, the cell utilizes the methanol to produce formaldehyde.[36] At an appropriate potential, the formaldehyde undergoes oxidation on the nanoparticle network (electrode) to form CO and H^+ and releases an electron per molecule of HCOH.[37,38] Analogous to cyclic voltametry,[39] the electron production leads to a maxima at $\sim$2 V attributed to (diffusion limited) oxidation current (Figure 6a). During the "down" cycle, from 10 to 0 V, no reduction-current is observed at $\sim$2 V as the product, CO, is a gas. However, the current is higher than "no yeast" because of variation in the quenched charge distribution due to redox electrons. In the reverse bias, the formaldehyde reduces to methanol[40] leading to a redox peak at ca. −3 V. In contrast, the device without the yeast cells shows an *I*−*V* behavior similar to Figure 3a as seen in Figure 6a ("no yeast"). It should be noted in passing that since the reactions are in solid state with no reference electrode, the redox peaks do not correspond to thermodynamic electrochemical potentials and change from sample to sample. The methanol exposure is performed by simply placing the device in a small sealed bell jar with a reservoir of methanol. The high currents are because the width of the network is $\sim$1 mm (in contrast to $\sim$100 μm for the device in Figure 3) to ensure deposition of yeast cells on the network. As a control, Figure 6a also shows the effect of formaldehyde vapor exposure on the *I*−*V* of a 10 μm device without the yeast cells (solid line in Figure 6a). A shoulder is observed close to the peak for the yeast seeded sample in forward bias while the behavior in reverse bias is similar. As there are no reference electrodes the physical nature of formaldehyde source (yeast *versus* vapor) is different, and the two curves for formaldehyde exposure (*i.e.*, with and without yeast) are on different chips, the comparison is reasonable and indicates that the *I*−*V* behavior is due to redox processes.

To demonstrate biogating, a constant bias of 4 V is applied to the cell−network device, and the current is monitored as the system is exposed to methanol (Figure 6b). A gain of approximately 5-fold is observed on exposure to methanol at P and Q in Figure 6b. After a couple of cycles, the yeast-network device is left at zero bias for $\sim$12 h in a humid environment. On subse-

quent methanol exposure, the gain reduces; and the rise time further slows down from ~20 to over 30 min. The slow rise is due to the response of the cell which is consistent with metabolic kinetics. At fixed bias of 4 V, the current modulation of approximately 5-fold observed in Figure 6b is consistent with Figure 6a, that is, an increase from points A to B. As a control, exposing the 10 μm device without yeast to methanol, a decrease (rather than increase as observed in Figure 6b) in current is observed (Figure S4 in Supporting Information). The observed biogating behavior in Figure 6b is explained as follows. Upon exposure to methanol, the electron, due to oxidation, alters the quenched charge distribution of the network, thereby modulating the current, similar to gating by a physical third electrode.[1] It is noted that (unfortunately) because the redox current quickly becomes inhibited by diffusion, the current gain to C does not occur (during biogating). The gain is due to the switching, that is, biogating, caused by the redistribution of quenched charge distribution from A to B.

SUMMARY

The fabrication process and device applications of a 2D network of 1D nanoparticle necklaces has been described. Mediated by mobile ions on the nanoparticle surface, the particles self-assemble in solution to form long necklaces that can be directly deposited onto electrical circuitry. The local 1D conductor nature of the array leads to fundamental differences in its behavior of V_T as a function of T. In previously reported studies on conducting 2D nanoparticle arrays, V_T decreases linearly with increasing temperature and vanishes at room temperature; however, for the network described herein, the slope abruptly flattens above ~50 K. The insensitivity to T above 50 K produces single-electron switching at room temperature in the array. The effect is attributed to barricades of single particles with single-electron charge embedded in the 1D necklace segment above 50 K.

For the first time, biogating using the metabolism of a living cell using a single-electron device has been demonstrated. The response time of the device to the chemical stimulation is consistent with the kinetics of the cell's metabolism. The possibility of measuring biochemical processes in the cell by biogating will potentially lead to applications in bioenergy, using the network as electrodes, and high sensitivity biosensors, where the subtle modulation in current, due to change in single-electron charge distribution caused by adsorption of biomolecules, viruses, microorganisms, or cells, can be measured in real time.

Acknowledgment. R.F.S. would like to thank the National Nanotechnology Initiative of the National Science Foundation, Award CMMI 0926381, and the Office of Basic Sciences, DOE, Award DE-SC0001302, for financial support. We would also like to thank the Biological Processing Development Facility (BPDF) at the University of Nebraska for providing the yeast cells.

Supporting Information Available: Preparation of the nanoparticle necklace, optical spectrum of the necklace suspension in aqueous media, and determination of V_T from $I-V$ data. This material is available free of charge *via* the Internet at http://pubs.acs.org.

REFERENCES AND NOTES

1. Likharev, K. K. Single-Electron Devices and Their Applications. *Proc. IEEE* **1999**, *87*, 606–632.
2. Klein, D. L.; Roth, R.; Lim, A. K. L.; Alivisatos, A. P.; Mceuen, P. L. A Single-Electron Transistor Made from a Cadmium Selenide Nanocrystal. *Nature* **1997**, *389*, 699–701.
3. Persson, S. H. M.; Olofsson, L.; Gunnarsson, L. A Self-Assembled Single-Electron Tunneling Transistor. *Appl. Phys. Lett.* **1999**, *74*, 2546–2548.
4. Berven, C. A.; Clarke, L.; Mooster, J. L.; Wybourne, M. N.; Hutchison, J. E. Defect-Tolerant Single-Electron Charging at Room Temperature in Metal Nanoparticle Decorated Biopolymers. *Adv. Mater.* **2001**, *13*, 109–113.
5. Averin, D. V.; Korotkov, A. N. Correlated Single-Electron Tunneling Via Mesoscopic Metal Particles—Effects of the Energy Quantization. *J. Low Temp. Phys.* **1990**, *80*, 173–185.
6. Berven, C. A.; Wybourne, M. N.; Clarke, L.; Longstreth, L.; Hutchison, J. E.; Mooster, J. L. Background Charge Fluctuations and the Transport Properties of Biopolymer-Gold Nanoparticle Complexes. *J. Appl. Phys.* **2002**, *92*, 4513–4517.
7. Middleton, A. A.; Wingreen, N. S. Collective Transport in Arrays of Small Metallic Dots. *Phys. Rev. Lett.* **1993**, *71*, 3198–3201.
8. Ancona, M. G.; Kruppa, W.; Rendell, R. W.; Snow, A. W.; Park, D. Coulomb Blockade in Single-Layer Au Nanocluster Films. *Phys. Rev. B* **2001**, *64*, 033408.
9. Blunt, M. O.; Šuvakov, M.; Pulizzi, F.; Martin, C. P.; Pauliac-Vaujour, E.; Stannard, A.; Rushforth, A. W.; Tadić, Bosiljka; Moriarty, P. Charge Transport in Cellular Nanoparticle Networks: Meandering through Nanoscale Mazes. *Nano Lett.* **2007**, *7*, 855–860.
10. Parthasarathy, R.; Lin, X. M.; Jaeger, H. M. Electronic Transport in Metal Nanocrystal Arrays: The Effect of Structural Disorder on Scaling Behavior. *Phys. Rev. Lett.* **2001**, 87 Art. No. 186807.
11. Black, C. T.; Murray, C. B.; Sandstrom, R. L.; Sun, S. H. Spin-Dependent Tunneling in Self-Assembled Cobalt-Nanocrystal Superlattices. *Science* **2000**, *290*, 1131–1134.
12. DeVries, G. A.; Brunnbauer, M.; Hu, Y.; Jackson, A. M.; Long, B.; Neltner, B. T.; Uzun, O.; Wunsch, B. H.; Stellacci, F. Divalent Metal Nanoparticles. *Science* **2007**, *315*, 358–361.
13. Huang, J. X.; Kim, F.; Tao, A. R.; Connor, S.; Yang, P. D. Spontaneous Formation of Nanoparticle Stripe Patterns through Dewetting. *Nat. Mater.* **2005**, *4*, 896–900.
14. Rabani, E.; Reichman, D. R.; Geissler, P. L.; Brus, L. E. Drying-Mediated Self-Assembly of Nanoparticles. *Nature* **2003**, *426*, 271–274.
15. Markovich, G.; Collier, C. P.; Henrichs, S. E.; Remacle, F.; Levine, R. D.; Heath, J. R. Architectonic Quantum Dot Solids. *Acc. Chem. Res.* **1999**, *32*, 415–423.
16. Narayanan, S.; Wang, J.; Lin, X. M. Dynamical Self-Assembly of Nanocrystal Superlattices during Colloidal Droplet Evaporation by *in Situ* Small Angle X-ray Scattering. *Phys. Rev. Lett.* **2004**, *93*, 135503.
17. Berry, V.; Saraf, R. F. Self-Assembly of Nanoparticles on Live Bacterium: An Avenue to Fabricate Electronic Devices. *Angew. Chem., Int. Ed.* **2005**, *44*, 6668–6673.
18. Parthasarathy, R.; Lin, X. M.; Elteto, K.; Rosenbaum, T. F.; Jaeger, H. M. Percolating through Networks of Random Thresholds: Finite Temperature Electron Tunneling in Metal Nanocrystal Arrays. *Phys. Rev. Lett.* **2004**, *92*, 076801.
19. Braun, E.; Eichen, Y.; Sivan, U.; Ben-Yoseph, G. DNA-Templated Assembly and Electrode Attachment of a Conducting Silver Wire. *Nature* **1998**, *391*, 775–778.

20. Patolsky, F.; Weizmann, Y.; Lioubashevski, O.; Willner, I. Au-Nanoparticle Nanowires Based on DNA and Polylysine Templates. *Angew. Chem., Int. Ed.* **2002**, *41*, 2323–2327.
21. Ugarte, D.; Chatelain, A.; deHeer, W. A. Nanocapillarity and Chemistry in Carbon Nanotubes. *Science* **1996**, *274*, 1897–1899.
22. Minko, S.; Kiriy, A.; Gorodyska, G.; Stamm, M. Mineralization of Single Flexible Polyelectrolyte Molecules. *J. Am. Chem. Soc.* **2002**, *124*, 10192–10197.
23. Jiang, K. Y.; Eitan, A.; Schadler, L. S.; Ajayan, P. M.; Siegel, R. W. Selective Attachment of Gold Nanoparticles to Nitrogen-Doped Carbon Nanotubes. *Nano Lett.* **2003**, *3*, 275–277.
24. Kumar, A.; Pattarkine, M.; Bhadbhade, M.; Mandale, A. B.; Ganesh, K. N.; Datar, S. S.; Dharmadhikari, C. V.; Sastry, M. Linear Superclusters of Colloidal Gold Particles by Electrostatic Assembly on DNA Templates. *Adv. Mater.* **2001**, *13*, 341–344.
25. Warner, M. G.; Hutchison, J. E. Linear Assemblies of Nanoparticles Electrostatically Organized on DNA Scaffolds. *Nat. Mater.* **2003**, *2*, 272–277.
26. Bae, A. H.; Numata, M.; Hasegawa, T.; Li, C.; Kaneko, K.; Sakurai, K.; Shinkai, S. 1D Arrangement of Au Nanoparticles by the Helical Structure of Schizophyllan: A Unique Encounter of a Natural Product with Inorganic Compounds. *Angew. Chem., Int. Ed.* **2005**, *44*, 2030–2033.
27. Fu, X. Y.; Wang, Y.; Huang, L.; Sha, Y.; Gui, L.; Lai, L.; Tang, Y. Assemblies of Metal Nanoparticles and Self-Assembled Peptide Fibrils—Formation of Double Helical and Single-Chain Arrays of Metal Nanoparticles. *Adv. Mater.* **2003**, *15*, 902.
28. Tlusty, T.; Safran, S. A. Defect-Induced Phase Separation in Dipolar Fluids. *Science* **2000**, *290*, 1328–1331.
29. Tang, Z. Y.; Kotov, N. A.; Giersig, M. Spontaneous Organization of Single CdTe Nanoparticles into Luminescent Nanowires. *Science* **2002**, *297*, 237–240.
30. Lin, S.; Li, M.; Dujardin, E.; Girard, C.; Mann, S. One-Dimensional Plasmon Coupling by Facile Self-Assembly of Gold Nanoparticles into Branched Chain Networks. *Adv. Mater.* **2005**, *17*, 2553–2559.
31. Maheshwari, V.; Kane, J.; Saraf, R. F. Self-Assembly of a Micrometers-Long One-Dimensional Network of Cemented Au Nanoparticles. *Adv. Mater.* **2008**, *20*, 284–287.
32. Hong, M.; Wu, L. L.; Tian, L. F.; Zhu, J. Controlled Assembly of An, Ag, and Pt Nanoparticles with Chitosan. *Chem.—Eur. J.* **2009**, *15*, 5935–5941.
33. Maier, S. A.; Kik, P. G.; Atwater, H. A.; Meltzer, S.; Harel, E.; Koel, B. E.; Requicha, A. A. G. Local Detection of Electromagnetic Energy Transport below the Diffraction Limit in Metal Nanoparticle Plasmon Waveguides. *Nat. Mater.* **2003**, *2*, 229–232.
34. Elteto, K.; Antonyan, E. G.; Nguyen, T. T.; Jaeger, H. M. Model for the Onset of Transport in Systems with Distributed Thresholds for Conduction. *Phys. Rev. B* **2005**, *71*, 064206.
35. Geigenmuller, U.; Schon, G. Single Electron Effects in Arrays of Normal Tunnel Junctions. *Europhys. Lett.* **1989**, *10*, 765–770.
36. Sibirny, A. A.; Titorenko, V. I.; Gonchar, M. V.; Ubiyvovk, V. M.; Ksheminskaya, G. P.; Vitvitskaya, O. P. Genetic Control of Methanol Utilization in Yeasts. *J. Basic Microbiol.* **1988**, *28*, 293–319.
37. Korpan, Y. I.; Gonchar, M. V.; Sibirny, A. A.; Martelet, C.; El'skaya, A. V.; Gibson, T. D.; Soldatkin, A. P. Development of Highly Selective and Stable Potentiometric Sensors for Formaldehyde Determination. *Biosens. Bioelectron.* **2000**, *15*, 77–83.
38. ten Kortenaar, M. V.; Kolar, Z. I.; de Gopeij, J. J. M.; Frens, G. Electrocatalytic Oxidation of Formaldehyde on Gold Studied by Differential Electrochemical Mass Spectrometry and Voltammetry. *J. Electrochem. Soc.* **2001**, *148*, E327−E335.
39. Bard, A. J. Faulkner, L. R. *Electrochemical Methods: Fundamentals and Applications.* J. Wiley & Sons: New York, 2001.
40. Montenegro, M. I.; Pletcher, D.; Liolios, E. A.; Mazur, D. J.; Zawodzinski, C. A Microelectrode Study of the Reduction of Formaldehyde in Neutral Concentrated Aqueous-Solutions. *J. Appl. Electrochem.* **1990**, *20*, 54–59.